Acceleration of corrosion of 304 stainless steel by outward extracellular electron transfer of Pseudomonas aeruginosa biofilm

Huang, Luyao; Chang, Weiwei; Zhang, Dawei; Huang, Ye; Li, Ziyu; Lou, Yuntian; Qian, Hongchang; Jiang, Chengying; Li, Xiaogang; Mol, Arjan

DOI
10.1016/j.corsci.2022.110159

Publication date
2022

Document Version
Final published version

Published in
Corrosion Science

Corrosion Science 199 (2022) 110159

Contents lists available at ScienceDirect

Corrosion Science

journal homepage: www.elsevier.com/locate/corsci

Acceleration of corrosion of 304 stainless steel by outward extracellular electron transfer of *Pseudomonas aeruginosa* biofilm

Luyao Huang [a,b,c,1], Weiwei Chang [a,c,1], Dawei Zhang [a,c,d,*], Ye Huang [e], Ziyu Li [f], Yuntian Lou [a,c], Hongchang Qian [a,c,d], Chengying Jiang [e], Xiaogang Li [a,c,d], Arjan Mol [f]

[a] Beijing Advanced Innovation Center for Materials Genome Engineering, Institute for Advanced Materials and Technology, University of Science and Technology Beijing, Beijing, China
[b] State Key Laboratory of Advanced Power Transmission Technology, Global Energy Interconnection Research Institute Co., Ltd, China
[c] National Materials Corrosion and Protection Data Center, University of Science and Technology Beijing, Beijing, China
[d] BRI Southeast Asia Network for Corrosion and Protection (MOE), Shunde Graduate School of University of Science and Technology Beijing, Foshan 528399, China
[e] State Key Laboratory of Microbial Resources, Institute of Microbiology, Chinese Academy of Sciences, Beijing, China
[f] Delft University of Technology, Department of Materials Science and Engineering, Mekelweg 2, Delft 2628CD, The Netherlands

ARTICLE INFO

Keywords:
Microbiological corrosion
Stainless steel
Pseudomonas aeruginosa
Extracellular electron transfer

ABSTRACT

The influence of outward extracellular electron transfer (EET) of *Pseudomonas aeruginosa* in accelerating corrosion of 304 stainless steel was investigated. With less NO_3^- available as electron acceptor, *P. aeruginosa* biofilm accelerated the pitting corrosion. The ICP-MS and XPS results indicated that *P. aeruginosa* promoted the bioreductive dissolution of iron oxides in the passive film of stainless steel. Using in situ scanning electrochemical microscopy, we established a relationship between this accelerated deterioration of the passive film and the EET process mediated by the conversion of the redox states of pyocyanin secreted by *P. aeruginosa*.

1. Introduction

Microbial biofilms are ubiquitous in most of atmospheric, soil and seawater environments and also many industrial environments related to infrastructure, marine transportation and oil exploitation [1]. Once biofilms are established on a metal surface, high cellular density present in the biofilm facilitates the competition for nutrients and other resources on the surface, and induces changes in the physicochemical properties of solution-metal interface, such as pH variation, O_2 gradient and ion diffusivity [2,3]. These changes may lead to the deterioration of metals and cause severe corrosion damage, known as microbiologically influenced corrosion (MIC) [4].

Extracellular electron transfer (EET) is a microbial metabolism that enables efficient electron transfer between microbial cells and extracellular solid materials. EET has received considerable attention for diverse microbial electrochemical applications, including pollutant mineralization, microbial fuel cell (MFC) and environmental biosensing [5,6]. Besides, numerous studies revealed that some microorganisms stimulate iron corrosion via EET metabolisms, which has been considered a prevalent MIC mechanism that promotes corrosion of metals [7–9]. Two different electron transfer strategies have been proposed in typical EET processes. One is direct electron transfer (DET), which relies on specific transmembrane proteins with redox activities (membrane-bound c-type cytochromes) and/or conductive nanowires (pili) [10–12]; the other is mediated electron transfer (MET), which is enabled via redox-active molecules (also known as electron shuttles) such as flavins secreted by *Shewanella* spp. and phenazines by *Pseudomonas* spp. [13,14]. The EET process could be divided into the outward EET (from the bacteria to electrode) and the inward EET (from the electrode to bacteria), according to the direction in which electrons transfer from the perspective of the bacteria [15]. The outward EET is generally conducted at the “bioanode”, where the extracellular electrode is served as the electron acceptor. In comparison, the inward EET is generally conducted at the “biocathode”, where the electrode is served as the electron donor [16].

Up to date, most studies have reported that microorganisms accelerate corrosion of metallic materials via inward EET by which microbial biocathodes could uptake electrons from Fe(0) anodes. For example,

* Corresponding author at: Beijing Advanced Innovation Center for Materials Genome Engineering, Institute for Advanced Materials and Technology, University of Science and Technology Beijing, Beijing, China.
E-mail address: dzhang@ustb.edu.cn (D. Zhang).
[1] These authors contributed equally to this work.

https://doi.org/10.1016/j.corsci.2022.110159
Received 11 June 2021; Received in revised form 28 January 2022; Accepted 4 February 2022
Available online 9 February 2022

Dinh et al. [17] isolated two sulfate-reducing bacteria (SRB) strains from marine sediment using metallic iron as the sole electron donor. Venzlaff et al. [18] proposed that direct electron uptake rather than microbial metabolite H_2S accelerated the corrosion of pure iron. Deposited FeS as a semiconductor may mediate electron transfer between metal and cells. Furthermore, Gu et al. [19] suggested that bacteria in the pre-established *Desulfovibrio vulgaris* biofilms became more corrosive under organic carbon source starvation since they switched from organic carbon oxidation to Fe(0) oxidation in order to obtain energy for growth. *Geobacter sulfurreducens* is another kind of electroactive microorganism which has been found to extract electrons from steel and lead to broader and deeper corrosion pits on 304L stainless steel [20]. Tang et al. [21] constructed a mutant *G. sulfurreducens* strain ACL_{HF} by deleting the genes for the uptake of hydrogenase and formate dehydrogenases. With this strain ACL_{HF}, the authors excluded the possibility of H_2 or formate serving as electron carriers and directly proved that electron transfer from Fe(0) can support anaerobic respiration and promote corrosion. Philips et al. [22] isolated a *Shewanella* strain 4t3–1–2LB from an acetogenic community enriched with Fe(0) as the sole electron donor. Compared with the corrosion rate in sterile medium, strain 4t3–1–2LB induced a 7-fold increase of the corrosion rate with fumarate as electron acceptor.

Pseudomonas aeruginosa is one of the most important bacteria in natural environment in consideration of its ability to serve pioneer bacteria to form complex biofilms on different types of metals [23]. Numerous laboratory studies have shown that *P. aeruginosa* biofilm can lead to deterioration of different steels via inward EET [24–26]. Recently, studies, using *P. aeruginosa* mutant strain incapable of secreting phenazines derivatives pyocyanin (PYO) and phenazine-1–carboxamide (PCN) as electron transfer mediators, have confirmed the significant role of phenazines in regulating EET of *P. aeruginosa* in MIC [27,28]. Phenazines are a kind of secondary metabolite produced by *P. aeruginosa* [13]. Conjugated bonds presented in heterocyclic aromatic rings of phenazines is considered to be the molecular origin of redox activity at appropriate reduction potentials [29]. Therefore, they could serve as electron transfer mediators and transfer electrons inward or outward crossing the cell membrane [30]. In an inward EET process, phenazines, especially PYO, can transfer electrons released from Fe(0) oxidation to the interior of *P. aeruginosa* cells for the reduction of electron acceptors. Unlike inward EET which is already used to explain MIC particularly for steels, outward EET mediated by phenazines of *P. aeruginosa* are more often reported in applications such as MFC and bioremediation [31]. For example, Hernandez et al. [32] found that multiple phenazines can function as electron shuttles and reduce insoluble ferric iron to Fe^{2+}. Yong et al. [33] constructed a *P. aeruginosa* mutant strain with *phzM* gene overexpressing. The *phzM* overexpression strain exhibited a 1.6 fold increase in PYO production, which greatly improved the EET efficiency and the electricity power output of *P. aeruginosa* MFC. However, whether and how this outward EET would induce or accelerate corrosion remains largely unexplored.

Herein, the role of outward EET by electron transfer mediator PYO in MIC of stainless steels caused by *P. aeruginosa* was investigated by varying the concentration of NO_3^- in the medium. The Fe^{III} compounds in the passive film of stainless steels and NO_3^- could both serve as electron acceptors to compete for the electrons released from bacteria. The difference in the MIC rates under gradient culture conditions were demonstrated by the corrosion morphology, pit topography and statistics and electrochemical measurements. The surface composition and the semiconducting property of the passive film were investigated by X-ray photoelectron spectroscopy (XPS). The dissolved metallic ions from the coupons and the production of phenazine derivatives were measured via high performance liquid chromatography (HPLC) analysis and inductively coupled plasma mass spectrometry (ICP-MS). Scanning electrochemical microscopy (SECM) was employed for in situ mapping of the redox states of PYO during the MIC caused by *P. aeruginosa*.

2. Experimental method

2.1. Bacterium, medium, and materials

The wild type *P. aeruginosa* (WT) (MCCC 1A00099) used in this study was obtained from the Marine Culture Collection of China (MCCC), Xiamen, China. The *P. aeruginosa* knockout mutant strain (Δ*phzM*+Δ*phzS*) with genes *phzM* and *phzS* knockout were generated by using a modified polymerase chain reaction-driven overlap extension strategy described in our previous work [28].

Ferrocenylmethanol (FcMeOH) was purchased from Yuanye Biotechnology Co., Ltd. Na-succinate was obtained from Shanghai Macklin Biochemical Co., Ltd. Na_2SeO_4 was purchased from Shandong Xiya Chemical Industry Co., Ltd. All other chemical reagents were purchased from Oxoid and Sinopharm Chemical Reagent Co., Ltd. All chemicals were used as purchased without further purification.

Frozen glycerol stocks (−80 °C) of WT were revived in aerobic Luria-Bertani (LB) medium (containing 10 g/L tryptone, 5 g/L yeast extract, and 10 g/L NaCl) and grown overnight at 37 °C with shaking at 150 rpm. Immersion and electrochemical tests were carried out in a minimal media (14.15 mM KH_2PO_4, 38.85 mM K_2HPO_4, 42.8 mM NaCl, 9.3 mM NH_4Cl, 40 mM Na-succinate and 40/10/0 mM KNO_3), in which Na-succinate and KNO_3 were provided to serve as the electron donor and the electron acceptor, respectively. The minimal media were neutralized to pH 7.2 and autoclaved at 121 °C for 20 min (MLS-3781-PC, Panasonic, Japan). Filter-sterilized SL-10 trace element solution (1 mL) and $MgSO_4$ (1 mM) were added to the media after autoclaving [34]. The media were then purged with the filter-sterilized N_2 for 2 h to remove dissolved oxygen. All the anaerobic manipulations were conducted in an anaerobic chamber (Thermo Fisher Scientific 1029, USA) filled with N_2.

304 stainless steel coupons with an upper exposed surface area of 1 cm^2 were used for the immersion and electrochemical tests. Before use, the coupons were all wet-abraded sequentially with a series of abrasive papers (240, 400, 800, and 1500 grit), and were subsequently ultrasonically rinsed with deionized water for 15 min. Prior to MIC tests, all coupons were sterilized with 75% ethanol and dried under ultraviolet irradiation in anaerobic chamber for 30 min. To obtain mature biofilms on the coupon surfaces, three replicate steel coupons were added into a conical flask containing 100 mL LB medium and 2 mL culture at an initial bacterial concentration of 1×10^6 cells/mL, and incubated at 37 °C for 2 days. After the 2-day pre-growth period, the coupons were removed and rinsed three times with phosphate buffer saline (PBS) (pH 7.4). The coupons were then placed into 100 mL serum bottles with 50 mL of the aforementioned anaerobic media. The serum bottles were then sealed with rubber stoppers and incubated at 37 °C for 7 days. The measurements on the 304 stainless steel in the sterile medium with 40 mM NO_3^- served as the control in this study.

2.2. Bacteria growth test

The planktonic cell counts under different electron acceptor (NO_3^-) levels were checked every day during the 7-day incubation. For the sessile cell counts, the specimens were gently rinsed with PBS to remove the non-adherent bacteria and immediately transferred to sterile centrifuge tubes containing 2 mL of PBS. Then the samples were washed by ultrasonic cleaning to collect the attached cells on the surface. Subsequently, the PBS solution were vortexed for 30 s to distribute cells evenly in the solution before counting. A haemocytometer under a light microscope (Lab A1, Zeiss) at 400× magnification was used to calculate the numbers of sessile cells. The pH of the culture medium was measured in triplicate with a pH meter (S220-B, Mettler Toledo). All tests for the bacteria growth measurements were performed in triplicate and the error bars reflected the mean deviation.

2.3. Biofilm characterization

For scanning electron microscope (SEM – Quanta 250, FEI, USA) observation of the surface morphology, the coupons were taken out from the media and gently rinsed with PBS to remove the non-adherent cells after the immersion tests. The coupons were then fixed with 2.5% glutaraldehyde in 0.1 M PBS solution for 4 h at 4 °C. They were then washed 3 times in 0.1 M PBS solution at 4 °C for 10 min and dehydrated in successive ethanol-water mixtures of 50%, 60%, 70%, 80%, 90%, 95%, and 100% (v/v) for 8 min [35]. Samples were further air dried and sputter-coated with gold to improve surface conductivity.

2.4. Surface analysis

Before measurement, the corrosion product and biofilm were removed from the coupons surface by derusting solution (ISO 8407: 2009, IDT) through ultrasonic cleaning for 2 min. The derusting solution contained 100 mL nitric acid, 20 mL hydrofluoric acid and 880 mL deionized water. Then, the depth and width of the corrosion pits on the steel surface were measured by confocal laser scanning microscopy (CLSM, VK-X, Keyence, Japan). The maximum pit depth was determined by averaging the deepest 10 pits from each coupon surface (total of three coupons). The error bars reflected the mean deviation. XPS analysis was performed on the coupons after the immersion tests using an XPS analyzer (ESCALAB 250Xi, Thermo Fisher Scientific, USA). Before XPS tests, the WT biofilm was removed from the coupon surface with sterile cotton swabs immediately after the coupons were taken out, followed by rinsing with deionized water twice, dried by purging with nitrogen gas, and finally stored in an air-tight vacuum desiccator prior to XPS analysis [36]. To obtain the depth profiles of the alloying elements, the surface (analyzed area of 700 × 300 μm^2) was sputtered by Ar^+ ion bombardment with an ion beam of 1 kV, a sample current of 1 μA, a step size of 0.1 eV, and a sputtering rate of 0.2 nm/s. All the XPS peaks were corrected to standard carbon C 1s binding energy of 284.8 eV. The XPS results were analyzed by the software XPS Peak (Version 4.1). The FWHM of the peaks were controlled in a reasonable range of 0.5–2.5 eV. The L/G ratios were set at a fixed value of 0.2. The XPS measurements were performed in triplicate and only one representative curve was displayed.

2.5. Electrochemical measurements

All electrochemical measurements were performed using a potentiostat (Reference 600^+, Gamry Instruments Inc, USA) and a standard three-electrode system consisting of the steel coupon (1 cm^2) as the working electrode, a standard calomel reference electrode (RE) and a platinum counter electrode (CE). The glassware was autoclaved at 121 °C for 20 min and the electrodes were sterilized with 75% (v/v) ethanol and dried under ultraviolet irradiation for 30 min prior to use. Open circuit potential (*OCP*) was first measured after immersing the coupons in the media with different concentrations of NO_3^-. Linear polarization resistance (LPR) was then measured in a potential range from −10–10 mV vs. *OCP* with the scanning rate of 0.125 mV/s. Electrochemical impedance spectroscopy (EIS) was performed with a 5 mV sinusoidal voltage vs. *OCP* and within the frequency range of 10^{-2} to 10^5 Hz [37]. EIS results were analyzed with ZSimDemo (EChem Software). We displayed one curve for the LPR and the EIS results, while the error bars reflected the reproducibility from triplicate measurements and showed the mean deviations. Mott-Schottky plots were obtained by scanning from 0.2 V_{SCE} towards a negative direction with a scanning rate of 20 mV/s and perturbation amplitude of 5 mV. The frequency (100 Hz) was selected based on the EIS data, such that the measured imaginary part of impedance is dominated by the capacitance of the passive film of the sample [37]. The Mott-Schottky test was carried out twice and we displayed one representative curve and the mean values of the donor concentration (N_D).

2.6. Chemical analyses

The dissolved metallic ions (Fe, Cr, and Ni) from the coupons were evaluated using ICP-MS (iCAP TQs ICP-MS, Thermo Fisher Scientific, USA). The biotic and abiotic media were pretreated with concentrated nitric acid and fed into the ICP-MS, which was operated at a nebulizer gas flow rate of 0.9941 L/min and an auxiliary gas flow rate of 0.7874 L/min. The transient signal was recorded with a dwell time of 0.02 s and a 50/e sweep number reading. The radio frequency power was 1550 W with a cool gas flow rate of 14 L/min.

The chemical compositions of the media were determined by means of ion chromatography (LC-2010Plus, Shimadzu, Japan) after centrifugation and filtration. The production of phenazine derivatives by each strain was measured via HPLC (LC-20 AD, Shimadzu, Japan) analysis according to the reported method [38]. Cultures were filtered (pore size 0.2 μm) and extracted three times with an equal volume of chloroform. After pooling and evaporating the solvent, the solid residue was dissolved in acetonitrile and subjected to C18 reversed-phase HPLC. HPLC effluent was monitored with a UV detector at 250 nm and 313 nm. All the ICP-MS and HPLC tests were repeated three times and the error bars reflected the mean deviation.

2.7. SECM measurements

For biofilm formation, the coupons were immersed in the LB medium containing WT and incubated aerobically for 2 days at 37 °C. After the pre-grown period, the coupons were washed twice with PBS to remove the non-adherent cells and then assembled to the SECM stage. The SECM setup is shown in Fig. S1. A high-resolution three-dimensional 3D positioning system was used to control the movement of the ultramicroelectrode (UME). The tip-biofilm (substrate) distance was fixed at ~20 μm with the aid of a negative feedback approach curve by using 1 mM FcMeOH as a redox mediator [39,40]. Cells were washed three times with PBS to remove any FcMeOH in the solution. Subsequently, 2 mL of supernatant from Δ*phzM*+Δ*phzS* was added to the chamber. Here, the supernatant produced by Δ*phzM*+Δ*phzS* was used to mimic the initial supernatant of the bacterial culture, which was removed after the measurement of the feedback approach curve in SECM. In our previous work, Δ*phzM*+Δ*phzS* was proved to lose its ability to produce PYO [28]. A copper heating plate is assembled to keep the whole apparatus at 37 °C, which is surrounded by the water bath. The time was set to zero when the temperature reached 37 °C.

All of the SECM measurements were conducted under N_2 environment by using a CHI 920D instruments (CH Instruments). The SECM measurements were performed with a three-electrode system consisting of the ultramicroelectrode (UME, a 10-μm Pt electrode) as the working electrode, a standard Ag/AgCl/KCl (3.0 M) RE and a Pt CE. The size of the tip was measured under an optical microscope to satisfy the demand and the cyclic voltammetry (CV) curve was plotted to verify the usability of the UME (Fig. S2). The SECM measurements were conducted on a scan area of 50 × 100 μm^2 and with a scan rate of 10 μm/s at 37 °C. The 304 stainless steel sample was left at *OCP* during experiments. The UME was first polarized at 0.1 V (oxidizing the reduced PYO at the tip) to map the concentration of the reduced PYO above the biofilm on the coupons. Similarly, the UME was then polarized at −0.4 V (reducing the oxidized PYO at the tip) to map the concentration of the oxidized PYO in the same region [41].

3. Results and discussion

3.1. Bacterial growth and biofilm observation

Fig. 1a shows the counts of the planktonic cells for different levels of electron acceptor (NO_3^-) during the 7-day incubation period. In the medium containing 40 mM NO_3^-, planktonic cells increased in number in the first 3 days, reaching a maximum of 4 × 10^8 cells/mL, and then

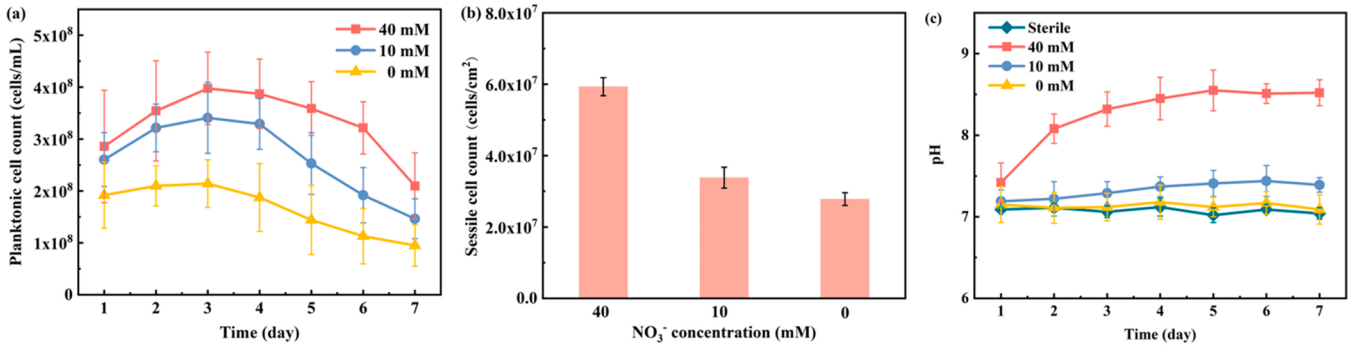

Fig. 1. (a) Planktonic cell counts during 7 days of immersion with 40 mM NO_3^-, 10 mM NO_3^- and 0 mM NO_3^-; (b) Sessile cell counts after 7 days of immersion with 40 mM NO_3^-, 10 mM NO_3^- and 0 mM NO_3^-; (c) pH variation of the abiotic control and the WT inoculated media with 40 mM NO_3^-, 10 mM NO_3^- and 0 mM NO_3^- during 7 days of immersion.

gradually decreased. After 7 days of incubation, the planktonic cell numbers reduced to 2.2×10^8 cells/mL. The results suggest that the reduction of the concentration of NO_3^- only had a small effect on the growth of the planktonic *P. aeruginosa* cells. In the media supplemented with 10 and 0 mM NO_3^-, planktonic cells presented a similar growth curve, with the counts of the planktonic cell being 1.7×10^8 and 1.0×10^8 cells/mL after 7 days, respectively. The counts of the sessile cells on the stainless steel surface after the 7-day incubation with different levels of NO_3^- are shown in Fig. 1b. The numbers of sessile cells in the presence of 10 and 0 mM NO_3^- were 3.2×10^7 and 2.7×10^7 cells/mL, respectively, both of which were much lower than the number of cells in the medium containing 40 mM NO_3^- (5.9×10^7 cells/mL). The pH variation of the WT inoculated media and the abiotic control over time is showed in Fig. 1c. When 40 mM NO_3^- was present in the medium, the pH values exhibited a slight increase in the first 3 days and thereafter stabilized at around 8.5, which may be attributed to the reduction of NO_3^- to NH_4^+ [42]. When only 10 mM NO_3^- was present, the pH values were maintained at ~7.3. When NO_3^- was completely removed in the medium, the pH value was ~7.2, which was close to that of the sterile control.

Fig. 2 shows the SEM images of the coupon surfaces after incubation with *P. aeruginosa* for 7 days. With 40 mM NO_3^- in the medium, a relatively dense biofilm was formed. The rod-shaped cells clustered together, covering most of the stainless steel surface. With 10 and 0 mM NO_3^- in the media, although the densities of the sessile cells were lower, sessile cells still migrated into clusters and attached to the steel surface. Biofilm morphologies observed by SEM were in accordance with sessile cells counts.

3.2. Pits observation and statistics

After 4 and 7 days of immersion in the abiotic control and the *P. aeruginosa* inoculated media with different initial NO_3^- concentrations, the average depth and density of the corrosion pits on the stainless steel surfaces are shown in Fig. 3. The corresponding pit morphology was presented in Fig. S3. No obvious pit was found on the samples from the sterile medium. With 40 mM NO_3^- in the medium, the average pit depths were 0.8 and 1.5 μm after 4 and 7 days, respectively. When the initial NO_3^- concentration decreased to 10 mM, the average depth and density of the corrosion pits both increased. On the surface of the coupons inoculated without NO_3^-, the average depth was 2.3 μm after 7 days of immersion. These results demonstrated that deep corrosion pits were most easily formed on the coupons in the media with 10 mM NO_3^-, followed by those in the media with 0 mM NO_3^- and 40 mM NO_3^-.

Fig. 4 shows the ionic leaching results from ICP-MS. The presence of WT induced a faster dissolution of Fe than that of Cr and Ni on the steel surface. After 7 days, the concentration of Fe ions was 53.12 μg/L in the

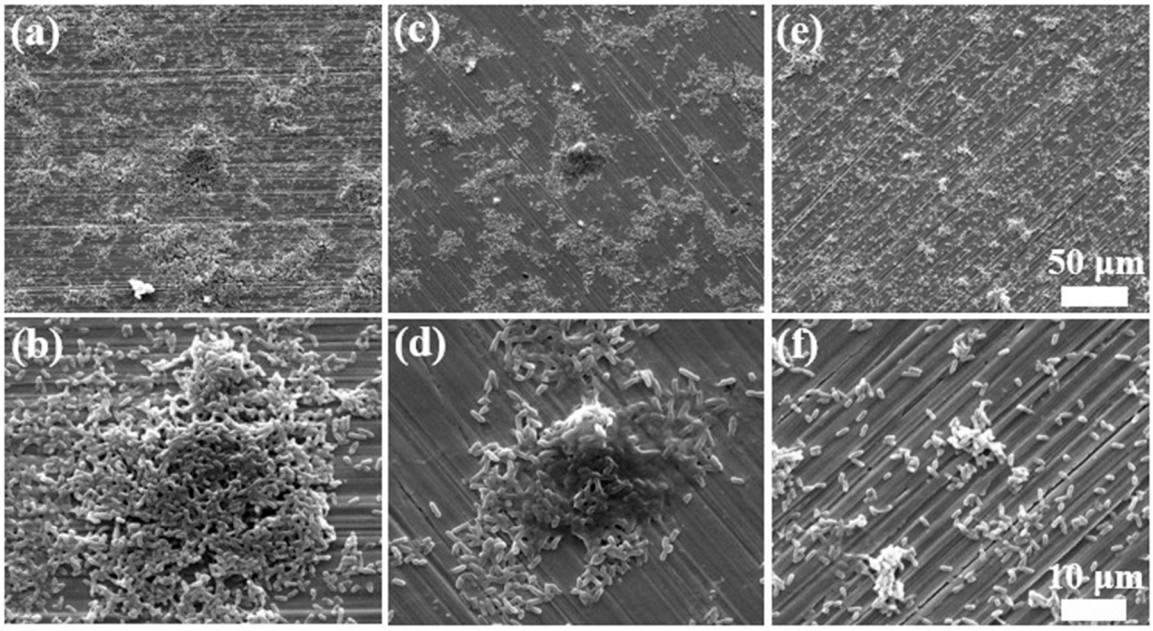

Fig. 2. SEM images of stainless steel surfaces after 7-day incubation in the *P. aeruginosa* inoculated media supplemented with (a, b) 40, (c, d) 10 or (e, f) 0 mM NO_3^-.

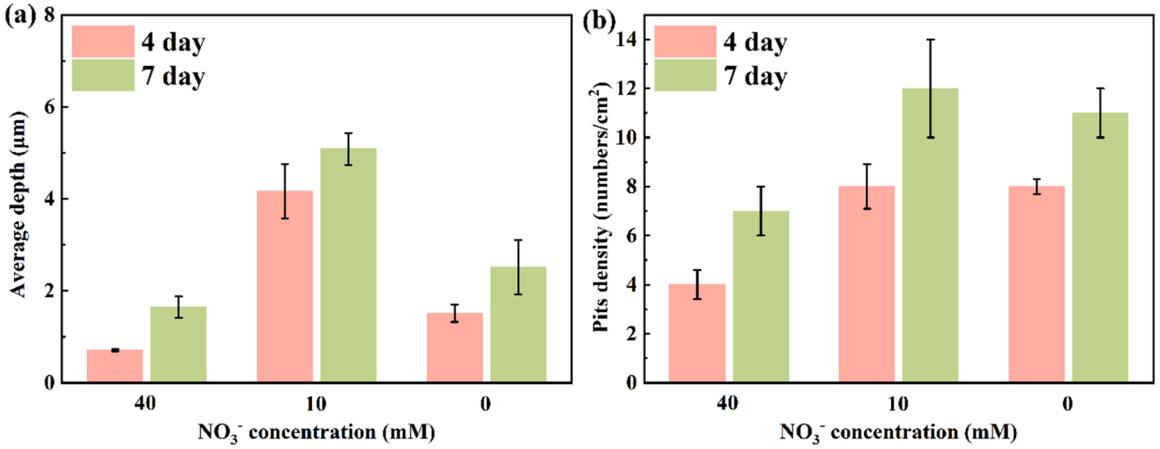

Fig. 3. (a) Average depth and (b) density of the corrosion pits on the stainless steel surfaces after 4 and 7 days of incubation in the media containing 40, 10 or 0 mM NO_3^-.

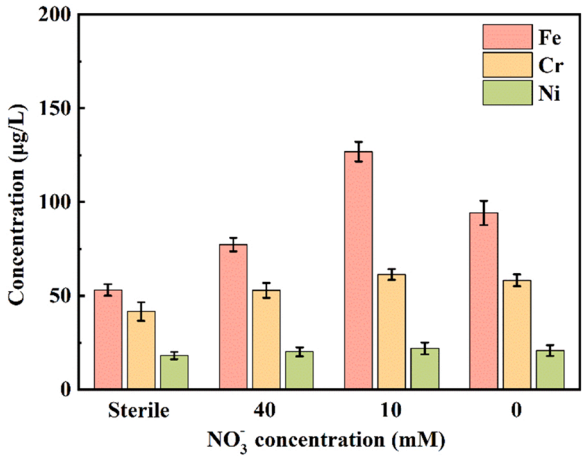

Fig. 4. ICP-MS results for the dissolved Fe, Cr and Ni in the sterile and WT inoculated media containing 40, 10 or 0 mM NO_3^-.

sterile medium. In comparison, the concentration of Fe ions reached 126.89 μg/L in the medium with 10 mM NO_3^-, which was nearly twice as high as that in the medium with 40 mM NO_3^- (77.29 μg/L). The concentration of Fe ions in the medium without NO_3^- (94.21 μg/L) was lower than that in the medium with 10 mM NO_3^- but still higher than that in the medium with 40 mM NO_3^-. At the same time, the amounts of dissolved Cr and Ni do not seem to be affected by the nitrate concentration.

3.3. XPS analysis

XPS analysis was performed to study the chemical composition of the passive film on the 304 stainless steel after immersion in the abiotic control and the WT inoculated media with different initial NO_3^- concentrations. The surface constituents and depth profiles of the passive film are both considered. Fig. 5 shows the detailed spectra of Fe $2p_{3/2}$, Cr $2p_{3/2}$ and O 1s. The corresponding binding energy of each compound is listed in Table S1. After immersion in the sterile medium, the proportions of Fe^0 and Cr^0 remained low. The Fe^{II}/Fe^{III} ratio and Cr_{ox}/Cr_{hy} ratio were 0.43 and 1.15 in the sterile medium, respectively. In Fig. 5a–d, the Fe $2p_{3/2}$ spectra obtained from the coupons inoculated with different concentrations of NO_3^- were deconvoluted into four constituents representing the metallic state Fe^0, oxide states Fe^{II} and Fe^{III}, and hydroxide state of Fe^{III}. The Fe^{II}/Fe^{III} ratio reached 0.97 for the sample inoculated with 40 mM NO_3^- and further increased to 1.51 and 1.09 for the samples inoculated with 10 mM and 0 mM NO_3^-, respectively. The reduction of the NO_3^- concentration promoted the reduction of Fe^{III} compounds in the passive film. As for the Cr $2p_{3/2}$ spectra, each spectrum can be fitted with three peak components, including Cr, Cr_2O_3 and $Cr(OH)_3$ (Fig. 5e–h). The Cr_{ox}/Cr_{hy} ratio in the coupons inoculated with WT were lower than that in the abiotic control. In general, a higher Cr_{ox}/Cr_{hy} ratio is beneficial for the stability of the passive film [43,44]. In the presence of 10 mM NO_3^-, the Cr_{ox}/Cr_{hy} ratio reached the minimum level, as the result of the decreased amount of Cr oxides and the increased amount of Cr hydroxides at the steel surface. This variation agrees well with the change of O_2^-/OH ratio which decreased from 0.84 to 0.42 and 0.51 as the NO_3^- concentration decreased from 40 mM to 10 mM and 0 mM, respectively. From the XPS analysis, the increased relative amounts of Fe^0 and Cr^0 and the decreased abundance of Fe^{III} (from both Fe^{III} oxides and Fe^{III} hydroxides) and Cr oxides compounds both suggested the thinning of the passive film and decreased passivity when less NO_3^- was available for *P. aeruginosa*.

To further investigate the effect of WT biofilm on the degradation of the passive film and the distribution of alloy elements, the surfaces of the coupons after immersion in the sterile control and the WT inoculated media were sputtered by Ar^+ ion bombardment every 5 s with an ion beam of 1 kV to obtain depth profiles of main elements in the passive films (Fig. 6). The continuous decrease of O content accompanied by the increase of Fe and Cr content with sputtering thickness (estimated based on the sputtering rate) is observed, revealing the transition from the surface film to the bulk steel. The thickness of the passive film is commonly determined as the sputtering depth at which O content was reduced to half relative to that at the sample surface [45]. The thickness of the passive film of the steel immersed in the sterile medium was 3.3 ± 0.2 nm (Fig. S4). The oxide film thickness decreased to 2.2 ± 0.3 nm for the sample inoculated with 40 mM NO_3^- and further decreased to 1.6 ± 0.1 and 2.0 ± 0.2 nm for the samples inoculated with 10 and 0 mM NO_3^-, respectively. The depth profiling results indicated that WT biofilm made the passive film thinner, especially in the culture media containing less NO_3^-. As the passive film becomes thinner, the pitting corrosion resistance of the 304 stainless steel decreases. The pit statistics support this conclusion.

3.4. Electrochemical measurements

Fig. 7 shows the Nyquist and Bode plots of the EIS results obtained after 4 and 7 days of immersion in abiotic control and in *P. aeruginosa* inoculated media supplemented with 40, 10 or 0 mM NO_3^-. For the coupons in abiotic control, the Nyquist plot showed a much larger partial semi-circle diameter compared to those obtained from the coupons in WT inoculated media and changed little during the whole

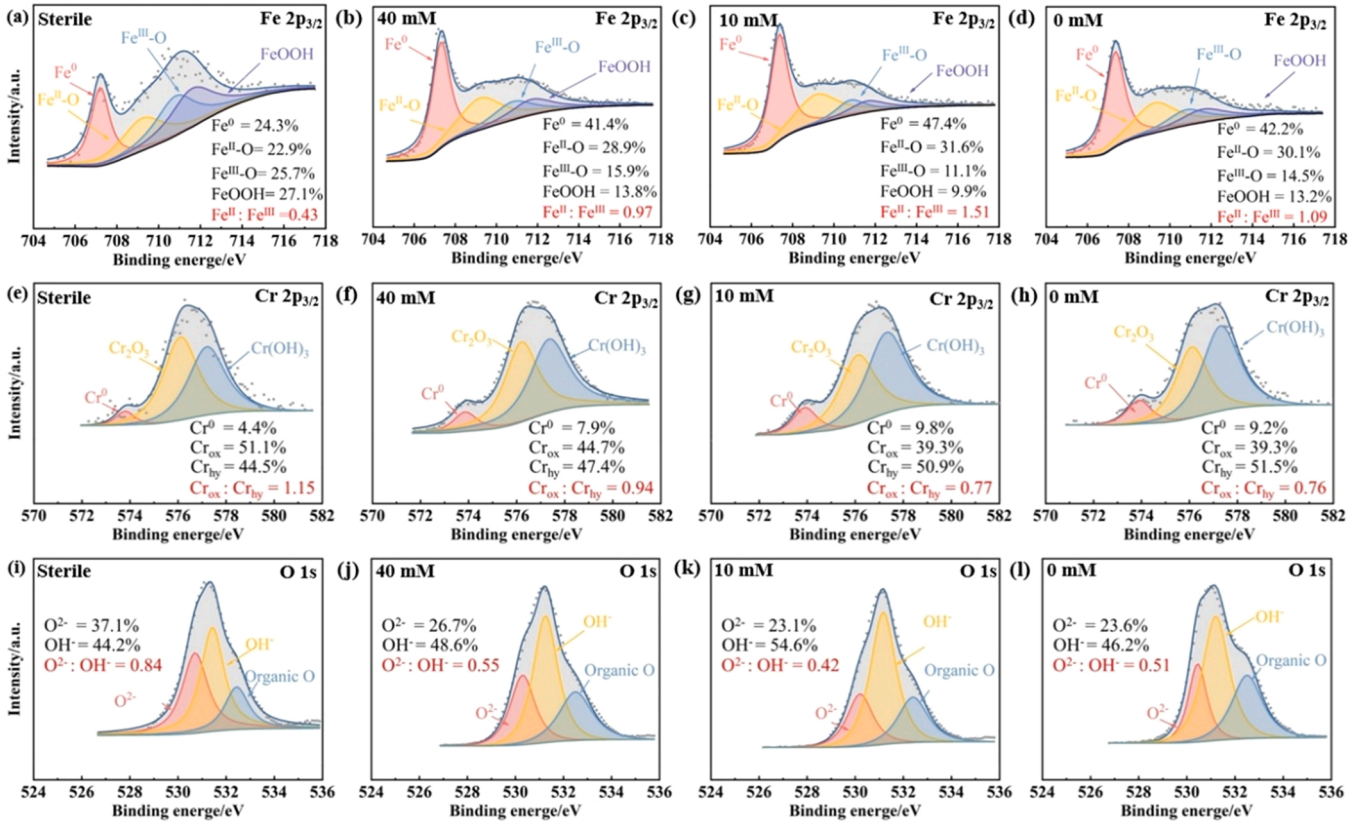

Fig. 5. High-resolution XPS spectra of Fe $2p_{3/2}$ (a–d), Cr$2p_{3/2}$ (e-h) and O1s (i–l) for the samples surfaces after immersion in the sterile control and the WT inoculated media with 40, 10 or 0 mM NO_3^- after 7 days of immersion.

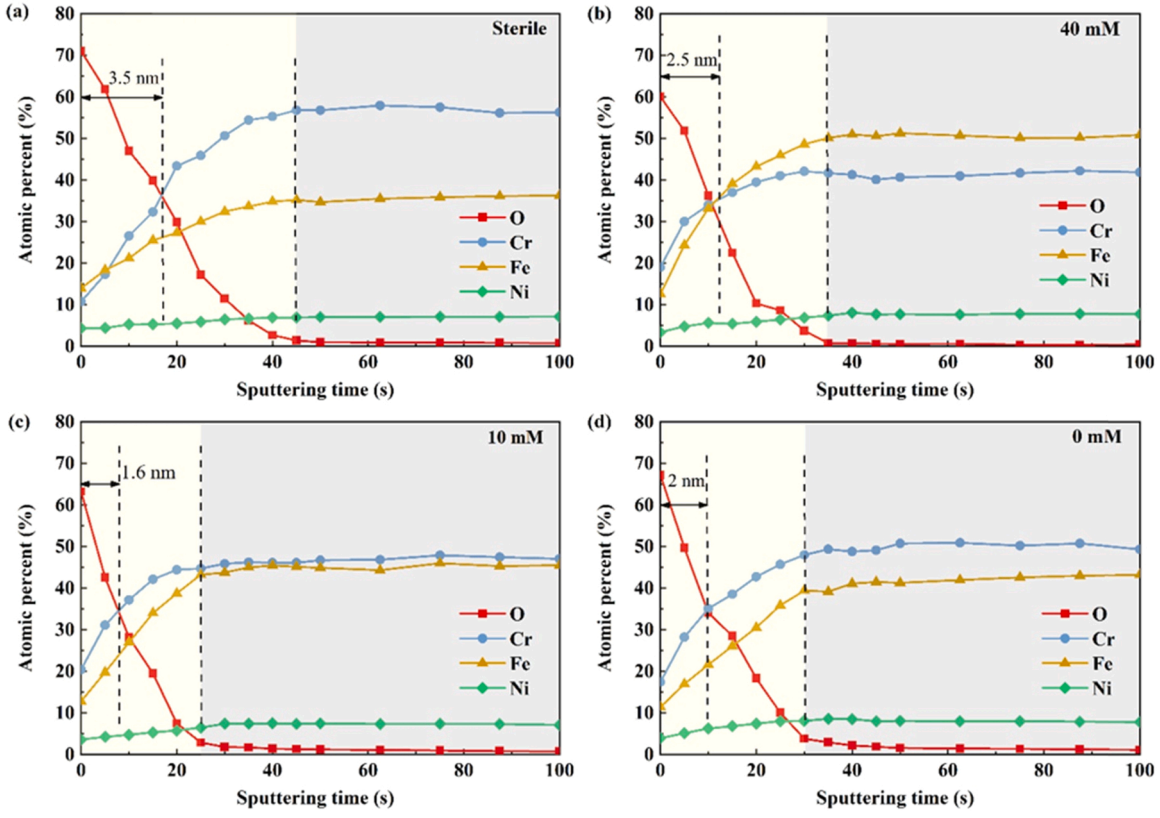

Fig. 6. XPS depth profiles of the main elements in the passive film of 304 stainless steel after immersion in the sterile medium and the WT inoculated media supplemented with 40, 10 or 0 mM NO_3^-.

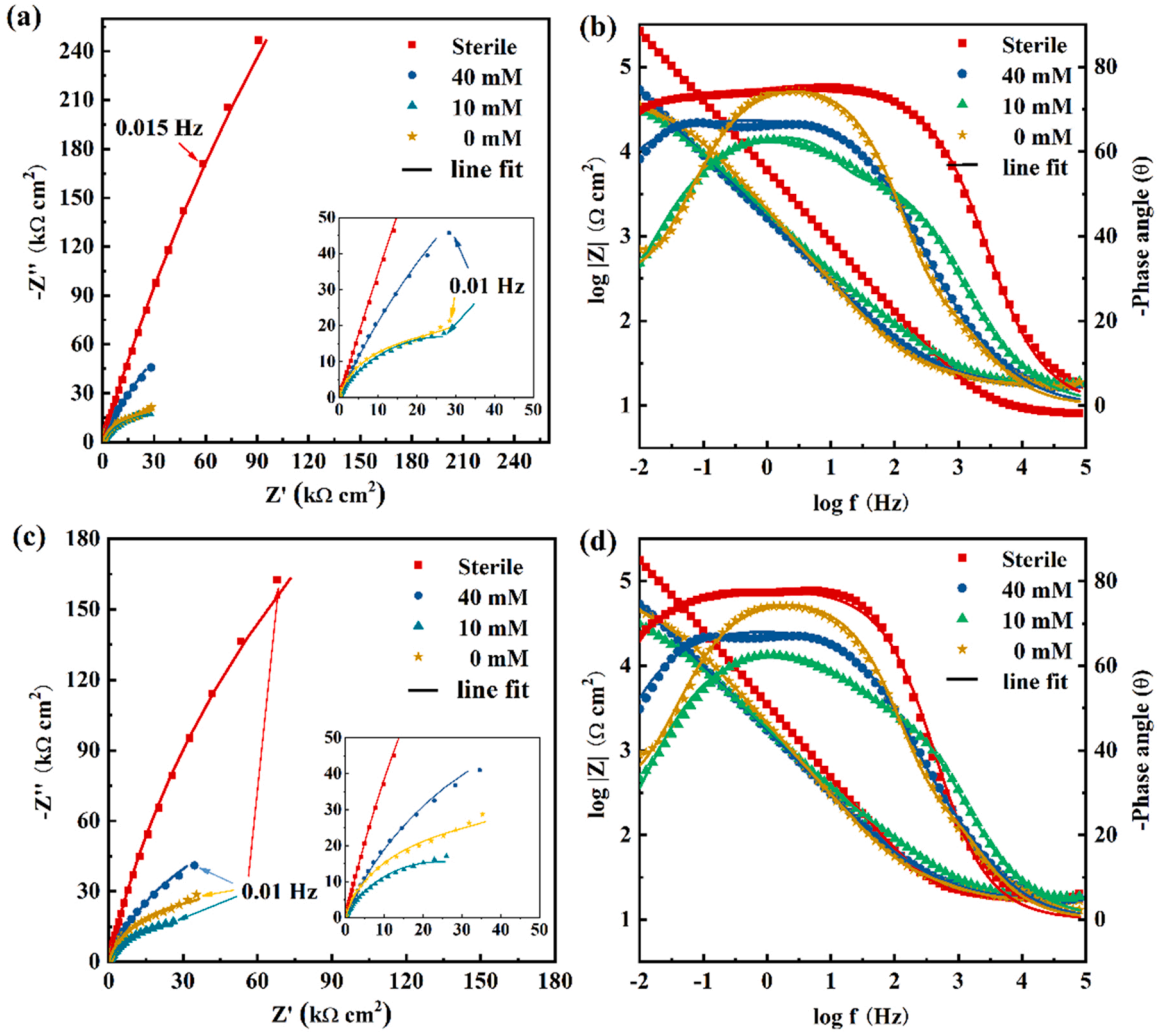

Fig. 7. Nyquist and Bode plots for the steels immersed in the sterile medium and the WT inoculated media supplemented with 40, 10 or 0 mM NO_3^- for (a, b) 4 and (c, d) 7 days.

immersion process. The corresponding Bode plot also presented relatively stable impedance modulus values in the low-frequency region ($|Z|_{0.01\ Hz}$), which is frequently used as a semi-quantitative indicator of the charge transfer resistance and hence corrosion resistance of the metal surface [46]. For the coupons in the WT inoculated media, the diameters of the Nyquist loops decreased significantly, confirming accelerated corrosion in the presence of the WT biofilm. The diameter of the Nyquist partial semi-circle was the smallest for the coupon in the medium containing 10 mM NO_3^- after 7 days of immersion. The $|Z|_{0.01\ Hz}$ values for the coupons immersed in the presence of different NO_3^- concentrations follow the order of 40 mM NO_3^- > 0 mM NO_3^- > 10 mM NO_3^-.

Two electrical circuit models were proposed to fit the EIS results. For the coupons in abiotic controls, a one-time constant model was used (Fig. 8a). The EIS results of the coupons immersed in the biotic groups were fitted well with two-time constant model (Fig. 8b). In the circuit, R_s is the resistance of the solution; Q_f and R_f represent the capacitance and resistance of the film composed of the *P. aeruginosa* biofilm and corrosion products layer, respectively; Q_{dl} and R_{ct} stand for the capacitance of the electrical double layer and the charge transfer resistance, respectively [47]. The constant phase elements Q are used instead of pure capacitance because of the non-ideal electrode surface, which is

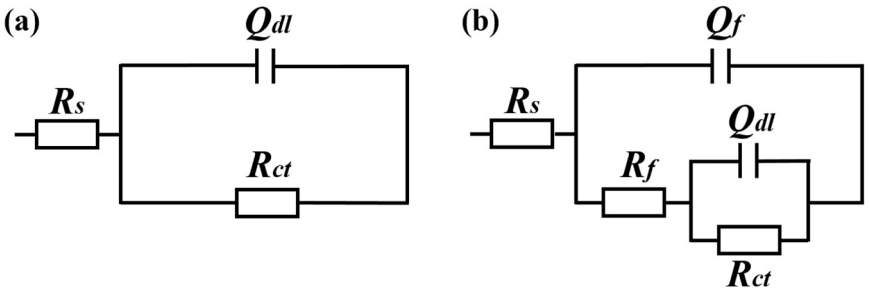

Fig. 8. The electrical equivalent circuit used to fit the EIS spectra.

particularly important for MIC considering the heterogenous nature of film composed of the *P. aeruginosa* biofilm and corrosion products layer [48]. Table 1 shows the corresponding fitting data. Among these parameters, R_{ct} is inversely proportional to corrosion rate, which is often used to reflect the electron transfer efficiency between the biofilm and metal surface [49]. The R_{ct} values for coupons in the sterile medium were larger than those in the presence of WT after the 7-day incubation. The R_{ct} value of the coupon in the inoculated medium containing 40 mM NO_3^- was 164.9 kΩ cm^2. With less NO_3^- in the media, R_{ct} values decreased to 48.2 kΩ cm^2 (10 mM NO_3^-) and 53.1 kΩ cm^2 (0 mM NO_3^-), suggesting a decreased corrosion resistance.

Fig. 9 presents the variation of the polarization resistance (R_p) determined from the LPR test on the coupons after immersion in abiotic control and in the WT inoculated media with 40, 10 or 0 mM NO_3^-. A higher R_p indicates better MIC resistance [50]. The highest R_p was shown for the samples immersed under abiotic condition. R_p values of the coupon in the absence of WT were stabilized around 450 kΩ cm^2. The R_p values for the coupons immersed in WT inoculated medium containing 10 and 0 mM NO_3^- were 38.7 and 54.3 kΩ cm^2, respectively, which were less than that of the coupon immersed in the medium containing 40 mM NO_3^- (157.1 kΩ cm^2). The results are in accordance with EIS results.

To further evaluate the degradation of the passive film of the stainless steel by *P. aeruginosa*, the semiconducting properties of the passive film were explored by Mott-Schottky analysis after immersing the coupons in the sterile control and the bacterial media with different NO_3^- concentrations for 7 days. According to Fig. 9b, the passive films formed on the 304 stainless steel show an n-type semiconducting property, which is due to the presence of $Fe(OH)_3$ and Fe_2O_3 in the passive film [51]. Based on the Mott-Schottky theory, the space charge capacitance (C) of a semiconductor can be calculated according to Eq. (1) [52]:

$$\frac{1}{C^2} = \frac{2}{\varepsilon\varepsilon_0 e N_D}\left(E\text{-}E_{FB}\text{-}\frac{kT}{e}\right) \quad (1)$$

in which N_D is the donor concentration; ε and ε_0 are the dielectric constant (generally 15.6) and the vacuum permittivity (8.8542×10^{-12} F/m), respectively; e is the electron charge (1.602×10^{-19} C); k is the Boltzmann constant (1.38×10^{-23} J/K); E and E_{FB} represent the applied potential and flat-band potential, respectively; and T is the absolute temperature (K). According to the slopes of the linear regions, the mean value of the corresponding charge carrier densities N_D in the passive film was calculated and shown in Fig. 9b. In the case of the passive films, the donors are primarily O vacancies in the oxide, so a higher N_D implies a more defective oxide film. After 7 days of immersion, N_D of the coupons immersed in the *P. aeruginosa* inoculated media was at the level of 10^{20} cm^{-3}, which is a typical value for passive films on stainless steels. In the medium containing 40 mM NO_3^-, N_D increased slightly and reached 7.1×10^{20} cm^{-3}. With 10 and 0 mM NO_3^- in the media, the N_D values increased to 1.3×10^{21} cm^{-3} and 1.1×10^{21} cm^{-3}, respectively, higher than that in the medium containing 40 mM NO_3^-. It is known that the formation and dissolution of Fe oxide are responsible for the change in the donor density; thus the increase in the donor density is related to the dissolution of the Fe^{III} in the passive film. The Mott-Schottky measurement results indicate that in general the passive film becomes more defective in the media with less NO_3^-.

3.5. HPLC analysis

For *P. aeruginosa*, phenazines usually serve as electron transfer mediators to mediate the EET of *P. aeruginosa* by carrying electrons inward or outward the cells. The variation of the concentrations of phenazines, including phenazine-1–carboxylate (PCA), PYO, PCN and 1–OH-phenazine (1–OH-PHZ) in the WT inoculated media with 40, 10 or 0 mM NO_3^- was measured by HPLC analysis. As shown in Fig. 10, WT secreted more PYO than PCA, PCN and 1–OH-PHZ. The concentration of secreted PYO in the inoculated medium was 1.56 μg/mL in the presence of 40 mM NO_3^-. When the concentrations of NO_3^- decreased to 10 mM and 0 mM, the concentrations of secreted PYO increased to 2.16 and 1.99 μg/mL, respectively. The variation of PCA concentration in the media showed a similar trend to that of PYO. The concentrations of both PCN and 1-OH-PHZ remained at much lower levels than that of PYO or PCA. These results confirmed that when the culture medium is lack of NO_3^- as soluble electron acceptor, WT can secrete more phenazines especially PYO and PCA which work as electron mediators to obtain energy from EET pathways.

3.6. SECM measurement

The reason why PYO plays important role in mediating the EET of WT *P. aeruginosa* biofilm is related to its feature to switch its redox state between an oxidized and a reduced state, which is governed by the half reaction [53]:

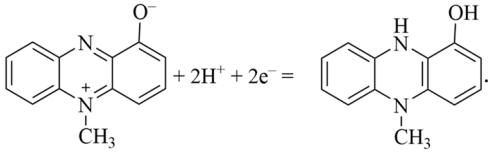

Reduced PYO has been shown to be able to reduce insoluble Fe(III) to soluble Fe(II), whereas the oxidized PYO often serves as an intermediate electron acceptor [32]. Thus, to better understand the significant role of PYO in MIC, it is of interest to monitor the variation of not only the concentration of PYO but also its redox state. SECM shows a significant potential for this type of investigation because of its ability to detect local variation of electrochemical information in the vicinity of the biofilm and to establish relationships between redox-active small molecules and the MIC process at the metal surface [54].

In this study, SECM measurements were performed at a constant height (20 μm) above the *P. aeruginosa* (both WT and Δ*phzM*+Δ*phzS*) biofilm on the steel surface. Based on a substrate generation/tip collection (SG/TC) operation mode, the reduced and oxidized PYO were detected at the UME tip by polarizing the UME tip at 0.1 V vs. Ag/AgCl (PYO oxidizing potential) and −0.4 V vs. Ag/AgCl (PYO reducing

Table 1
EIS parameters for the steels immersed in the sterile medium and the WT inoculated media supplemented with 40, 10 or 0 mM NO_3^-.

	R_s Ω cm^2	$Q_f \times 10^{-5}$ Ω^{-1} S^n cm^{-2}	R_f Ω cm^2	n_1	$Q_{dl} \times 10^{-5}$ Ω^{-1} S^n cm^{-2}	R_{ct} kΩ cm^2	n_2	$\chi^2 \times 10^{-4}$
4 day								
Sterile	8.2 ± 1.5	–	–	–	3.6 ± 0.7	1015.3 ± 100.9	0.83 ± 0.18	4.6 ± 0.8
40 mM	17.6 ± 2.8	9.1 ± 2.1	33.9 ± 6.2	0.71 ± 0.15	5.7 ± 0.7	375.1 ± 62.3	0.75 ± 0.12	7.5 ± 1.3
10 mM	17.3 ± 1.9	12.9 ± 1.8	122.3 ± 15.9	0.70 ± 0.11	0.9 ± 0.2	53.7 ± 6.4	0.95 ± 0.13	5.7 ± 1.5
0 mM	17.6 ± 3.1	4.1 ± 0.6	23.4 ± 3.8	0.86 ± 0.14	5.5 ± 0.7	58.3 ± 5.9	0.86 ± 0.16	9.4 ± 1.8
7 day								
Sterile	17.9 ± 2.2	–	–	–	5.8 ± 1.2	815.4 ± 42.5	0.87 ± 0.14	10.4 ± 2.9
40 mM	17.4 ± 3.7	9.4 ± 5.2	43.6 ± 8.8	0.77 ± 0.09	5.4 ± 0.9	164.9 ± 17.2	0.76 ± 0.09	8.4 ± 2.2
10 mM	18.1 ± 2.9	11.4 ± 2.6	47.3 ± 10.6	0.71 ± 0.12	3.6 ± 0.7	48.2 ± 8.9	0.80 ± 0.11	4.2 ± 1.1
0 mM	16.9 ± 4.2	14.9 ± 5.1	49.5 ± 11.1	0.79 ± 0.17	2.5 ± 0.5	53.1 ± 11.3	0.93 ± 0.13	11.3 ± 2.5

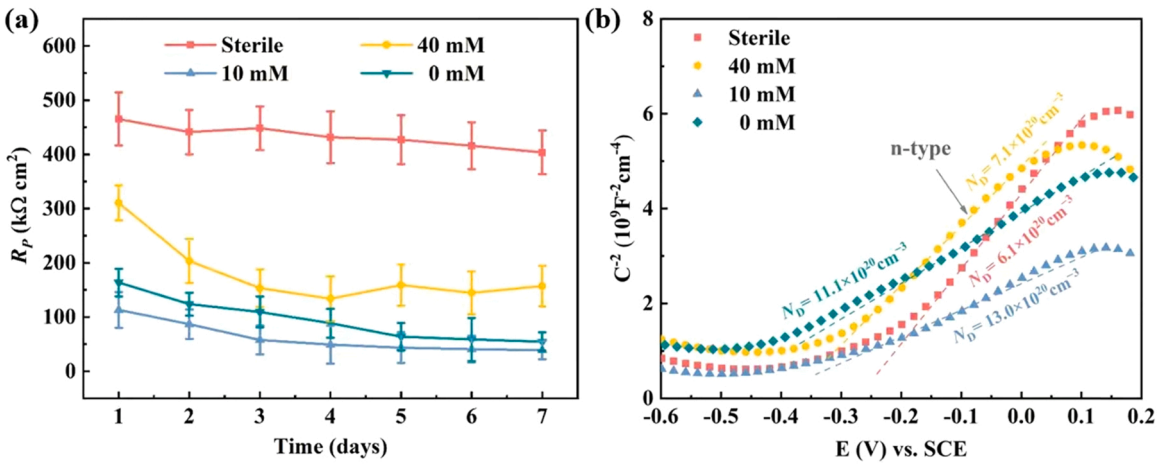

Fig. 9. (a) LPR results for the coupons in the sterile medium and the WT inoculated media containing 40, 10 or 0 mM NO_3^- during 7 days of immersion; (b) Mott-Schottky plots for the coupons after 7 days of immersion.

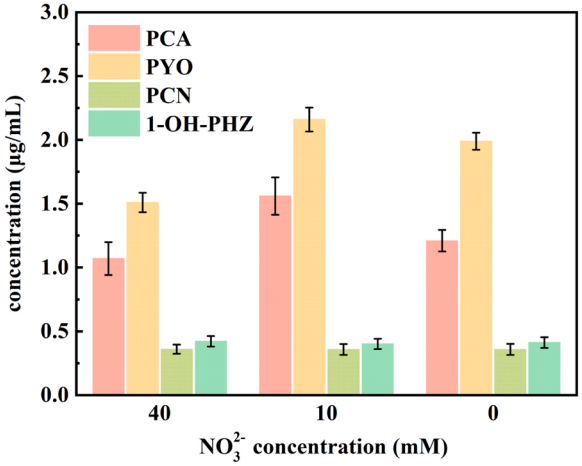

Fig. 10. Phenazine derivatives after immersion for 7 days in the WT inoculated media supplemented with 40, 10 or 0 mM NO_3^-.

potential) in the same region, respectively. As such, the interaction between the redox state of PYO and the stainless steel surface during the MIC process could be monitored in real time. Fig. 11 shows the level of current detected by the UME over the scanned surface. The red/yellow color and the blue color indicate the regions of low and high current, respectively. The green color refers to the base current. The magnitude of the current reflects the local concentration of the reactants (reduced or oxidized PYO). At 0.1 V, the presence of active regions above WT *P. aeruginosa* biofilm with lower current values indicated a decreased amount of the reduced PYO detected on the UME (Fig. 11a–c). At −0.4 V, a higher current distribution was observed in the same region, indicating that more reduced PYO was consumed by its interaction with the oxide passive film and converted into its oxidized form (Fig. 11a'–c'). In general, the higher local current values were observed for the samples in the presence of fewer NO_3^-, which agreed with the results of the aforementioned corrosion analyses. After knocking out *phzM* and *phzS* genes, the Δ*phzM*+ Δ*phzS* strain was no longer capable of producing PYO. Therefore, the SECM maps do not show local variation in the concentration of reduced PYO (Fig. 11d) or oxidized PYO (Fig. 11d'). The current variation influenced by *P. aeruginosa* on the passive film of 304 stainless steel is schematically illustrated in

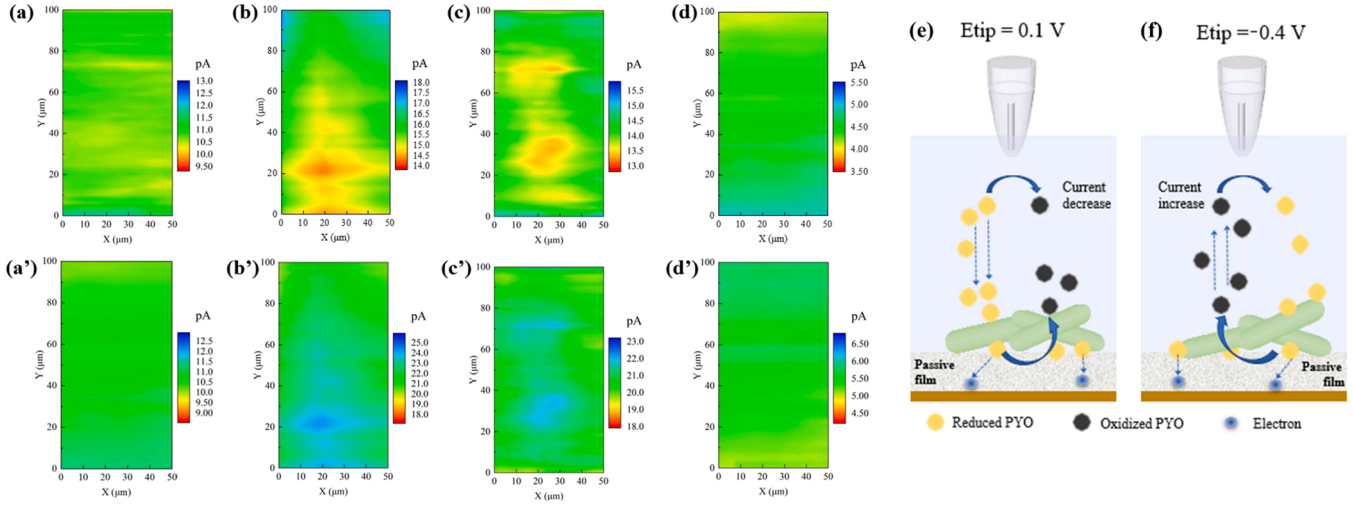

Fig. 11. *In situ* SECM imaging of steel surfaces after 12 h of immersion in media containing WT *P. aeruginosa* and Δ*phzM*+Δ*phzS P. aeruginosa*. The tip potential was set at 0.1 (a–d) and −0.4 V (a'–d') vs. Ag/AgCl to detect reduced PYO and oxidized PYO, respectively. Current mapping of reduced and oxidized PYO over 304 stainless steel surface covered with WT *P. aeruginosa* in the media containing (a, a') 40 mM NO_3^-, (b, b') 10 mM NO_3^-, (c, c') 0 mM NO_3^-. (d, d') Current mapping of reduced and oxidized PYO over 304 stainless steel surface covered with Δ*phzM*+Δ*phzS P. aeruginosa* in the media containing 40 mM NO_3^-. (e, f) Schematic of current variation influenced by *P. aeruginosa* on the passive film of 304 stainless steel surface.

(Fig. 11e–f).

In order to describe the conversion of the redox states of PYO more intuitively, as shown in Fig. 12, the ratio between the concentration of the reduced PYO and that of the oxidized PYO ($R_{re/ox}$) were calculated and mapped to depict the distribution of the redox state of PYO over the biofilm. The red/yellow colors indicate the regions with lower $R_{re/ox}$ values. In the presence of 40 mM NO_3^- (Fig. 12a), the $R_{re/ox}$ distribution of the reduced and oxidized PYO was relatively homogeneous over the biofilm surface, which suggested that the change of the redox state of PYO (as the result of interaction between bacteria and stainless steel) was small in the presence of abundant electron acceptors (NO_3^-) in the environment. When lower concentrations (10 and 0 mM) of NO_3^- were present (Fig. 12b,c), the SECM map exhibited a higher degree of heterogeneity in the distribution of $R_{re/ox}$, indicating more intense EET activities. In Fig. 12d, the $R_{re/ox}$ value remained homogeneous over the entire scanned area, which was attributed the inhibited secretion of PYO by the Δ*phzM*+Δ*phzS* biofilm.

4. Discussion

In this study, Na-succinate was the electron donor in the bacterial medium. Different amounts of initial NO_3^- were provided to serve as the soluble electron acceptor. With 40 mM NO_3^-, *P. aeruginosa* could utilize succinate as the electron donor and NO_3^- as the acceptor for cellular metabolism. Electron flow is diverted from ubiquinone to reduce NO_3^- to NO_2^- through the NapA nitrate reductase and further to N_2 and NH_4^+. The increased pH (8.51 after 7 days of immersion) could also be explained by this reduction reaction (Fig. 1). When the initial NO_3^- concentration was 10 mM, the soluble NO_3^- was not enough to support the bacterial growth during the immersion period. After 7 days, negligible NO_3^- (0.016 and 0.018 mM) were detected in the medium with 40 and 10 mM NO_3^-, respectively, which was far less than the initial concentration (Table S2). *P. aeruginosa* have to seek alternative electron acceptors for cellular metabolism when NO_3^- were completely consumed. Herein, the iron oxides in the passive film may serve as final electron acceptor and Fe^{III} are reduced to Fe^{II}, which deteriorates the passive film to resist pitting corrosion. The pit statistics showed that the WT biofilm caused accelerated pitting corrosion on the 304 stainless steel surfaces with a lower concentration of NO_3^-. Notably, the worst pitting occurred on the coupon surface immersed in the WT inoculated medium with 10 mM NO_3^-, rather than that with 0 mM NO_3^-. This may be attributed to the suppressed cell growth with the complete removal of NO_3^- in the culture medium. The results from XPS and electrochemical analyses further confirmed this accelerated pitting corrosion of 304 stainless steel via a PYO-mediated EET process of *P. aeruginosa*.

Unlike dissolved nitrate, iron oxides in stainless steel matrix are insoluble. Flow of electrons from the oxidation of succinate must be transported extracellularly to contact with iron oxides in the passive film. In *P. aeruginosa*, phenazines could be used as an electron transfer mediator and transfer electrons both inward or outward of the cell. In our previous work, PYO was proved to be an efficient electron transfer mediator to mediate the EET of *P. aeruginosa* by carrying electrons to cells [28]. The HPLC analysis also reveals that WT biofilms produce more PYO compared with other phenazines, especially in the media with 10 and 0 mM NO_3^-. Saunders et al. [14] proposed that extracellular eDNA is responsible for the interception of PYO, leading to the enrichment of PYO in *P. aeruginosa* biofilm to enable the sufficient electron transfer efficiency. The SECM measurements observed a similar heterogeneous distribution of reduced and oxidized PYO. Based on the SECM results, we proposed intracellular and extracellular electron transfer models. As illustrated in Fig. 13, electrons produced by the oxidation of succinate are transported through intracellular NAD^+/NADH and the ubiquinone pool (Q/QH_2). The electron flow is diverted from extracellular electron transfer chain to oxidized PYO in the *P. aeruginosa* cell, which turns into a reduced state and diffuses to the extracellular environment. When mature biofilm *P. aeruginosa* formed on the stainless steel surface, the reduced PYO contacts with iron oxides in the passive film and electrons are transferred from reduced PYO to iron oxides. Under this condition, insoluble Fe^{III} in the iron oxides is

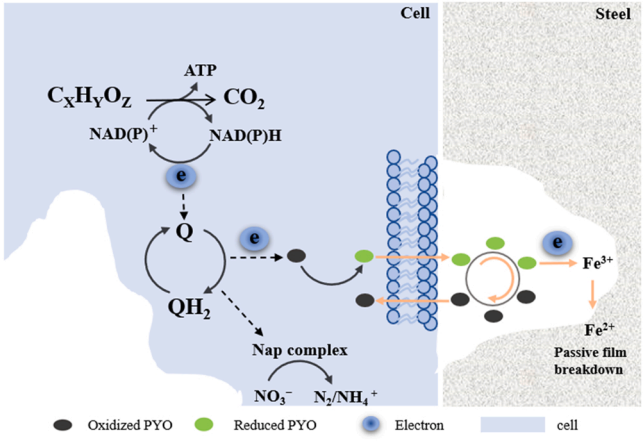

Fig. 13. Schematic diagram of the proposed EET models of electron flow from carbon source oxidation to extracellular Fe^{III} reduction. Dotted arrows indicate abbreviated or unknown electron transport steps.

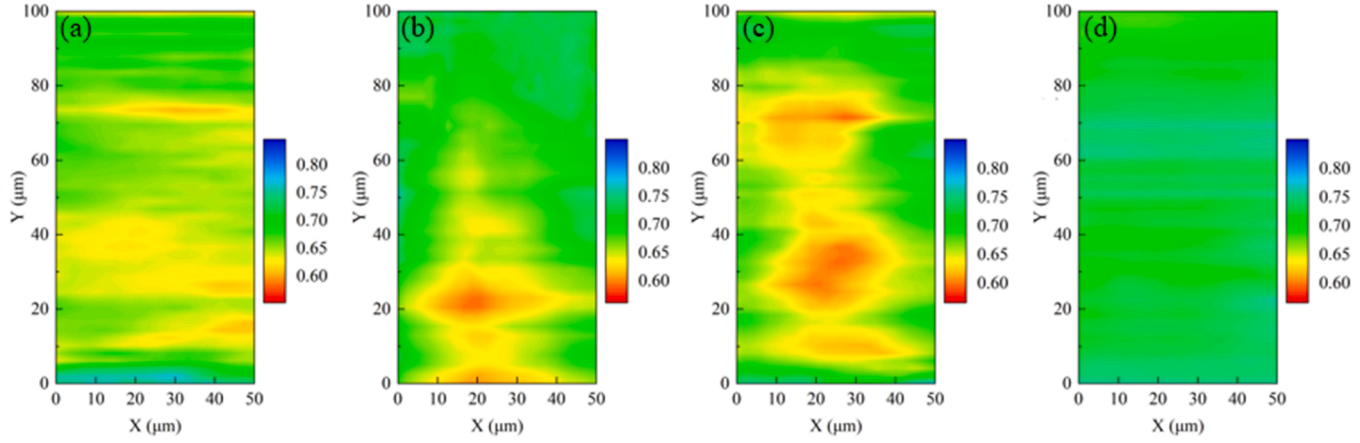

Fig. 12. Mapping of $R_{re/ox}$ values above WT and Δ*phzM*+Δ*phzS* biofilm on stainless steel surfaces after 12 h of immersion in media containing different concentration of NO_3^-. (a-c) $R_{re/ox}$ distribution above WT biofilm the in the media containing 40, 10, and 0 mM NO_3^-; (d) $R_{re/ox}$ distribution above Δ*phzM*+Δ*phzS* biofilm in the media containing 40 mM NO_3^-.

reduced to soluble Fe^{II}, and reduced PYO returns to the oxidized state. Through this outward MET process, the passive film of 304 stainless steel deteriorated. The results in Fig. 12 support this hypothesis showing that a lower $R_{re/ox}$ value and spatially more heterogeneous current distribution are observed upon decreasing NO_3^- concentration in a certain range. After knocking out *phzM* and *phzS* genes, the mutant strain was no longer capable of producing sufficient PYO to conduct the EET process between the Δ*phzM*+Δ*phzS* biofilm and stainless steel. The homogeneous current distribution with the Δ*phzM*+Δ*phzS* observed in the SECM image verified that the influence of biofilm morphology to the collection of tip current was limited.

According to this model, we have proposed the interaction between the EET process mediated by the conversion of the redox states of PYO of *P. aeruginosa* and an accelerated MIC process at the stainless steel surface. Through this outward MET process, bioreductive dissolution of iron oxides in passive film of stainless steel occurred, which promote the breakdown of passive film and further led to the occurring of pitting corrosion. The results in this study would help to understand how biofilms of electroactive bacteria could trigger the depassivation and localized corrosion of stainless steels in real environment. In the case that the environment lacks of suitable electron acceptors or that bacteria in the bottom of biofilm cannot capture enough electron acceptors due to the diffusion limitation and rapid consumption by the biofilm closer to the environment, the bacteria could accept electrons from the Fe^{III} compounds in the passive film and facilitate the pitting corrosion.

5. Conclusions

In this work, the influence of outward EET of *P. aeruginosa* in accelerating MIC of 304 stainless steel was investigated. *P. aeruginosa* biofilms incubated in the media containing lower levels of NO_3^- resulted in lower planktonic and sessile cell counts, yet accelerated pitting corrosion compared to those in the medium with 40 mM NO_3^-. ICP-MS and XPS results indicated a bioreductive dissolution of iron oxides in passive film of stainless steel. Using in situ SECM measurements, we have shown direct evidence that EET mediated by the conversion of the redox states of PYO of *P. aeruginosa* accelerated the deterioration of the passive film in stainless steel. This work provides strong evidence to clarify how EET is involved in the MIC of stainless steel by *P. aeruginosa* and shows that SECM can be used to study the redox reactions of EET process in MIC at a microelectrochemical scale.

CRediT authorship contribution statement

Luyao Huang: Conceptualization, Methodology, Investigation, Writing – original draft. **Weiwei Chang:** Investigation, Methodology, Writing – review & editing. **Dawei Zhang:** Supervision, Conceptualization, Methodology, Writing – original draft, Writing – review & editing. **Ye Huang:** Investigation. **Ziyu Li:** Conceptualization. **Yuntian Lou:** Investigation. **Hongchang Qian:** Investigation. **Chengying Jiang:** Methodology. **Xiaogang Li:** Supervision. **Arjan Mol:** Writing – review & editing. All authors contributed to the discussion of the work.

Declaration of Competing Interest

The authors declare that they have no known competing financial interests or personal relationships that could have appeared to influence the work reported in this paper.

Acknowledgment

This work was supported by the National Natural Science Foundation of China (52071015), the Open Fund from State Key Laboratory of Metal Material for Marine Equipment and Application (SKLMEA-K202006) and the Fundamental Research Funds for the Central Universities (FRF-BD-20-28A2).

Appendix A. Supporting information

Supplementary data associated with this article can be found in the online version at doi:10.1016/j.corsci.2022.110159.

References

[1] T. Bjarnsholt, M. Alhede, M. Alhede, S.R. Eickhardt-Sørensen, C. Moser, M. Kühl, P. Ø. Jensen, N. Høiby, The *in vivo* biofilm, Trends Microbiol 21 (2013) 466–474.
[2] L. Procópio, The role of biofilms in the corrosion of steel in marine environments, World J. Microbiol. Biotechnol. 35 (2019) 73.
[3] J.W. Costerton, The Biofilm Primer, Springer Berlin Heidelberg, 2007.
[4] B.J. Little, J.S. Lee, Microbiologically influenced corrosion: an update, Int. Mater. Rev. 59 (2014) 384–393.
[5] J.A. Gralnick, D.K. Newman, Extracellular respiration, Mol. Microbiol 65 (2007) 1–11.
[6] Y. Jiang, J.X. Zeng, Bidirectional extracellular electron transfers of electrode-biofilm: Mechanism and application, Bioresour. Technol. 271 (2019) 439–448.
[7] M. Mehanna, R. Basseguy, M.L. Deila, A. Bergel, Role of direct microbial electron transfer in corrosion of steels, Electrochem. Commun. 11 (2009) 568–571.
[8] S. Kato, Microbial extracellular electron transfer and its relevance to iron corrosion, Microb. Biotechnol. 9 (2016) 141–148.
[9] Y.T. Jin, Z. Li, E.Z. Zhou, Y. Lekbach, D.K. Xu, S.L. Jiang, F.H. Wang, Sharing riboflavin as an electron shuttle enhances the corrosivity of a mixed consortium of *Shewanella oneidensis* and *Bacillus licheniformis* against 316L stainless steel, Electrochim. Acta 316 (2019) 93–104.
[10] S. Pirbadian, S.E. Barchinger, K.M. Leung, H.S. Byun, Y. Jangir, R.A. Bouhenni, S. B. Reed, M.F. Romine, D.A. Saffarini, L. Shi, Y.A. Gorby, J.H. Golbeck, M.Y. El-Naggar, *Shewanella oneidensis* MR-1 nanowires are outer membrane and periplasmic extensions of the extracellular electron transport components, Proc. Natl. Acad. Sci. U. S. A 111 (2014) 12883–12888.
[11] B. Schuetz, M. Schicklberger, J. Kuermann, A.M. Spormann, J. Gescher, Periplasmic Electron Transfer via the c-Type Cytochromes MtrA and FccA of *Shewanella oneidensis* MR-1, Appl. Environ. Microbiol. 75 (2009) 7789–7796.
[12] D.J. Filman, S.F. Marino, J.E. Ward, L. Yang, Z. Mester, E. Bullitt, D.R. Lovley, M. Strauss, Cryo-EM reveals the structural basis of long-range electron transport in a cytochrome-based bacterial nanowire, Commun, Biol. 2 (2019) 219.
[13] N.R. Glasser, S.H. Saunders, D.K. Newman, The Colorful World of Extracellular Electron Shuttles, Annu. Rev. Microbiol. 71 (2017) 731–751.
[14] S.H. Saunders, E.C.M. Tse, M.D. Yates, F.J. Otero, S.A. Trammell, E.D.A. Stemp, J. K. Barton, L.M. Tender, D.K. Newman, Extracellular DNA promotes efficient extracellular electron transfer by pyocyanin in *pseudomonas aeruginosa* biofilms, Cell. 182 (2020) 919–932.
[15] T.Y. Gu, D. Wang, Y. Lekbach, D.K. Xu, Extracellular electron transfer in microbial biocorrosion, Curr Opin Electrochem 29 (2021), 100763.
[16] Z.Y. Li, W.W. Chang, T.Y. Cui, D.K. Xu, D.W. Zhang, Y.T. Lou, H.C. Qian, H. Song, A. Mol, F.H. Cao, T.Y. Gu, X.G. Li, Adaptive bidirectional extracellular electron transfer during accelerated microbiologically influenced corrosion of stainless steel, Commun. Mater. 67 (2021) 2.
[17] H.T. Dinh, J. Kuever, M. Mußmann, A.W. Hassel, M. Stratmann, F. Widdel, Iron corrosion by novel anaerobic microorganisms, Electrochem. Commun. 427 (2004) 829–832.
[18] D. Enning, H. Venzlaff, J. Garrelfs, H.T. Dinh, V. Meyer, K. Mayrhofer, A.W. Hassel, M. Stratmann, F. Widdel, Marine sulfate-reducing bacteria cause serious corrosion of iron under electroconductive biogenic mineral crust, Environ. Microbiol. 14 (2012) 1772–1787.
[19] D.K. Xu, T.Y. Gu, Carbon source starvation triggered more aggressive corrosion against carbon steel by the *Desulfovibrio vulgaris* biofilm, Int. Biodeterior. Biodegrad. 91 (2014) 74–81.
[20] M. Mehanna, R. Basseguy, M.L. Deila, R. Gubner, N. Sathirachinda, A. Bergel, Geobacter species enhances pit depth on 304L stainless steel in a medium lacking with electron donor, Electrochem. Commun. 11 (2009) 1476–1481.
[21] H.Y. Tang, D.E. Holmes, T. Ueki, P.A. Palacios, D.R. Lovley, Iron corrosion via direct metal-microbe electron transfer, MBio 10 (2019) e00303–e00319.
[22] J. Philips, N. van den Driessche, K. De Paepe, A. Prevoteau, J.A. Gralnick, J.B. A. Arends, K. Rabaey, A Novel *Shewanella* Isolate Enhances Corrosion by Using Metallic Iron as the Electron Donor with Fumarate as the Electron Acceptor, Appl. Environ. Microbiol. 84 (2018) e01154–18.
[23] H.W. Liu, Y.F. Cheng, Corrosion of X52 pipeline steel in a simulated soil solution with coexistence of *Desulfovibrio desulfuricans* and *Pseudomonas aeruginosa* bacteria, Corros. Sci. 173 (2020), 108753.
[24] Y. Zhao, E.Z. Zhou, D.K. Xu, Y.G. Yang, Y. Zhao, T. Zhang, T.Y. Gu, K. Yang, F. H. Wang, Laboratory investigation of microbiologically influenced corrosion of 2205 duplex stainless steel by marine *Pseudomonas aeruginosa* biofilm using electrochemical noise, Corros. Sci. 143 (2018) 281–291.
[25] Y.T. Lou, C.D. Dai, W.W. Chang, H.C. Qian, L.Y. Huang, C.W. Du, D.W. Zhang, Microbiologically influenced corrosion of FeCoCrNiMo0.1 high-entropy alloys by marine *Pseudomonas aeruginosa*, Corros. Sci. 165 (2019), 108390.
[26] R. Jia, D.Q. Yang, D.K. Xu, T.Y. Gu, Microbiologically influenced corrosion of C1018 carbon steel by nitrate reducing *Pseudomonas aeruginosa* biofilm under organic carbon starvation, Corros. Sci. 127 (2017) 1–9.
[27] Y. Huang, E.Z. Zhou, C.Y. Jiang, R. Jia, S.J. Liu, D.K. Xu, T.Y. Gu, F.H. Wang, Endogenous phenazine-1-carboxamide encoding gene *PhzH* regulated the

extracellular electron transfer in biocorrosion of stainless steel by marine *Pseudomonas aeruginosa*, Electrochem. Commun. 94 (2018) 9–13.
[28] L.Y. Huang, Y. Huang, Y.T. Lou, H.C. Qian, D.K. Xu, L.W. Ma, C.Y. Jiang, D. W. Zhang, Pyocyanin-modifying genes *phzM* and *phzS* regulated the extracellular electron transfer in microbiologically-influenced corrosion of X80 carbon steel by *Pseudomonas aeruginosa*, Corros. Sci. 164 (2020), 108355.
[29] G.P. Ren, Y. Sun, Y. Ding, A.H. Lu, Y. Li, C.Q. Wang, H.R. Ding, Enhancing extracellular electron transfer between *Pseudomonas aeruginosa* PAO1 and light driven semiconducting birnessite, Bioelectrochemistry 123 (2018) 233–240.
[30] Y. Wang, D.K. Newman, Redox reactions of phenazine antibiotics with ferric (hydr) oxides and molecular oxygen, Environ. Sci. Technol. 42 (2008) 2380–2386.
[31] H.B. Shen, X.Y. Yong, Y.L. Chen, Z.H. Liao, R.W. Si, J. Zhou, S.Y. Wang, Y.C. Yong, P.K. OuYang, T. Zhao, Enhanced bioelectricity generation by improving pyocyanin production and membrane permeability through sophorolipid addition in *Pseudomonas aeruginosa*-inoculated microbial fuel cells, Bioresour. Technol. 167 (2014) 490–494.
[32] M.E. Hernandez, A. Kappler, D.K. Newman, Phenazines and other redox-active antibiotics promote microbial mineral reduction, Appl. Environ. Microbiol. 70 (2004) 921–928.
[33] X.Y. Yong, D.Y. Shi, Y.L. Chen, J. Feng, X. Lu, J. Zhou, S.Y. Wang, Y.C. Yong, Y. M. Sun, P.K. OuYang, T. Zheng, Enhancement of bioelectricity generation by manipulation of the electron shuttles synthesis pathway in microbial fuel cells, Bioresour. Technol. 152 (2014) 220–224.
[34] R.M. Atlas. Handbook of Microbiological Media, Third Edition, CRC Press, 2004.
[35] J. Li, Z.Y. Liu, Y.T. Lou, C.W. Du, X.G. Li, Evidencing the uptake of electrons from X80 steel by *Bacillus licheniformis* with redox probe, 5-cyano-2,3-ditolyl tetrazolium chloride, Corros. Sci. 168 (2020), 108569.
[36] S.J. Yuan, S.O. Pehkonen, Microbiologically influenced corrosion of 304 stainless steel by aerobic *Pseudomonas* NCIMB 2021 bacteria: AFM and XPS study, Colloid Surf. B-Biointerfaces 59 (2007) 87–99.
[37] H.C. Qian, L.W. Ma, D.W. Zhang, Z.Y. Li, L.Y. Huang, Y.T. Lou, C.W. Du, Microbiologically influenced corrosion of 304 stainless steel by halophilic archaea *Natronorubrum tibetense*, J. Mater. Sci. Technol. 46 (2020) 12–20.
[38] R.O. Fernández, R.A. Pizarro, High-performance liquid chromatographic analysis of *Pseudomonas aeruginosa* phenazines, J. Chromatogr. A 771 (1997) 99–104.
[39] H.C. Qian, D.W. Zhang, T.Y. Cui, W.W. Chang, F.H. Cao, C.W. Du, X.G. Li, Accelerating effect of catalase on microbiologically influenced corrosion of 304 stainless steel by the halophilic archaeon *Natronorubrum tibetense*, Corros. Sci. 178 (2021), 109507.
[40] J. Kim, J.L. Connell, M. Whiteley, A.J. Bard, Development of a Versatile in Vitro Platform for Studying Biological Systems Using Micro-3D Printing and Scanning Electrochemical Microscopy, Anal. Chem. 86 (2014) 12327–12333.
[41] D. Koley, M.M. Ramsey, A.J. Bard, M. Whiteley, Discovery of a biofilm electrocline using real-time 3D metabolite analysis, Proc. Natl. Acad. Sci. U. S. A 108 (2011) 19996–20001.
[42] R. Jia, D.Q. Yang, D.K. Xu, T.Y. Gu, Electron transfer mediators accelerated the microbiologically influence corrosion against carbon steel by nitrate reducing *Pseudomonas aeruginosa* biofilm, Bioelectrochemistry 118 (2017) 38–46.
[43] X.Q. Yue, L. Zhang, C. Sun, S.S. Xu, C. Wang, M.X. Lu, A. Neville, Y. Hua, A thermodynamic and kinetic study of the formation and evolution of corrosion product scales on 13Cr stainless steel in a geothermal environment, Corros. Sci. 169 (2020), 108640.
[44] Y.P. Dou, S.K. Han, L.W. Wang, X. Wang, Z.Y. Cui, Characterization of the passive properties of 254SMO stainless steel in simulated desulfurized flue gas condensates by electrochemical analysis, XPS and ToF-SIMS, Corros. Sci. 165 (2020), 108405.
[45] X.Q. Yue, L. Zhang, Y. Wang, S.S. Xu, C. Wang, M.X. Lu, A. Neville, Y. Hua, Evolution and characterization of the film formed on super 13Cr stainless steel in CO_2-saturated formation water at high temperature, Corros. Sci. 163 (2020), 108277.
[46] S.Q. Chen, D. Zhang, Study of corrosion behavior of copper in 3.5 wt.% NaCl solution containing extracellular polymeric substances of an aerotolerant sulphate-reducing bacteria, Corros. Sci. 136 (2018) 275–284.
[47] H.W. Liu, C.Y. Fu, T.Y. Gu, G.A. Zhang, Y.L. Lv, H.T. Wang, H.F. Liu, Corrosion behavior of carbon steel in the presence of sulfate reducing bacteria and iron oxidizing bacteria cultured in oilfield produced water, Corros. Sci. 100 (2015) 484–495.
[48] F. Batmanghelich, L. Li, Y. Lee, Influence of multispecies biofilms of *Pseudomonas aeruginosa* and *Desulfovibrio vulgaris* on the corrosion of cast iron, Corros. Sci. 121 (2017) 94–104.
[49] Y.T. Hu, K. Xiao, D.W. Zhang, P. Yi, R.L. Xiong, C.F. Dong, J.S. Wu, X.G. Li, Corrosion acceleration of printed circuit boards with an immersion silver layer exposed to *Bacillus cereus* in an aerobic medium, Front. Microbiol. 10 (2019) 1493.
[50] H.C. Qian, D.W. Zhang, Y.T. Lou, Z.Y. Li, D.K. Xu, C.W. Du, X.G. Li, Laboratory investigation of microbiologically influenced corrosion of Q235 carbon steel by halophilic archaea *Natronorubrum tibetense*, Corros. Sci. 145 (2018) 151–161.
[51] Z.C. Feng, X.Q. Cheng, C.F. Dong, L. Xu, X.G. Li, Passivity of 316L stainless steel in borate buffer solution studied by Mott-Schottky analysis, atomic absorption spectrometry and X-ray photoelectron spectroscopy, Corros. Sci. 52 (2010) 3646–3653.
[52] N.E. Hakiki, M.F. Montemor, M.G.S. Ferreira, M. da Cunha, Belo, Semiconducting properties of thermally grown oxide films on AISI 304 stainless steel, Corros. Sci. 42 (2000) 687–702.
[53] J. Elliott, O. Simoska, S. Karasik, J.B. Shear, K.J. Stevenson, Transparent Carbon Ultramicroelectrode Arrays for the Electrochemical Detection of a Bacterial Warfare Toxin, Pyocyanin, Anal. Chem. 89 (2017) 6285–6289.
[54] R. Moreira, M.K. Schütz, M. Libert, B. Tribollet, V. Vivier, Influence of hydrogen-oxidizing bacteria on the corrosion of low carbon steel: Local electrochemical investigations, Bioelectrochemistry 97 (2014) 69–75.